J|A|C|S COMMUNICATIONS

Published on Web 03/17/2009

Flexible Pores of a Metal Oxide-Based Capsule Permit Entry of Comparatively Larger Organic Guests

Ayala Ziv,[†] Alina Grego,[†] Sivil Kopilevich,[†] Leila Zeiri,[†] Pere Miro,[‡] Carles Bo,[‡] Achim Müller,[§] and Ira A. Weinstock*,[†]

Department of Chemistry, Ben Gurion University of the Negev, Beer Sheva 84105, Israel, Institute of Chemical Research of Catalonia, Tarragona 43007, Spain, and Faculty of Chemistry, University of Bielefeld, D-33501 Bielefeld, Germany

Received January 20, 2009; E-mail: iraw@bgu.ac.il

In zeolites[1] and rigid functional materials,[2] substrates whose sizes exceed those of the pore dimensions are rigorously excluded. Meanwhile, cavities within flexible metal−organic frameworks (MOFs) can accommodate substrates by reversible, stepwise structural expansion ("breathing").[3] Now, using a "capsule-like" molybdenum oxide-based framework as a soluble analogue of porous solid-state (rigid) oxides, we find that branched-alkane "guests" can negotiate passage through flexible subnanometer Mo_9O_9 apertures whose geometrical dimensions are smaller than the entering species.

The parent complex for this work, **1** (Figure 1),[4] belongs to a family of molecular metal oxide-based coordination polymers with spherical periodicity[5,6] in which 12 pentagonal $\{(Mo^{VI})Mo^{VI}_5O_{21}(H_2O)_6\}^{6-}$ "ligands" are connected by 30 Cr^{3+}, Fe^{3+}, or $Mo^{V}_2O_4(acetate)^+$ "spacers". The structure of **1** with $Mo^{V}_2O_4(acetate)^+$ spacers contains 20 Mo_9O_9 rings that are ca. 3 Å in diameter on the basis of the van der Waals radii of opposing O atoms. These Mo_9O_9 rings serve as porelike openings to the interior of the water-soluble capsule-like complex.

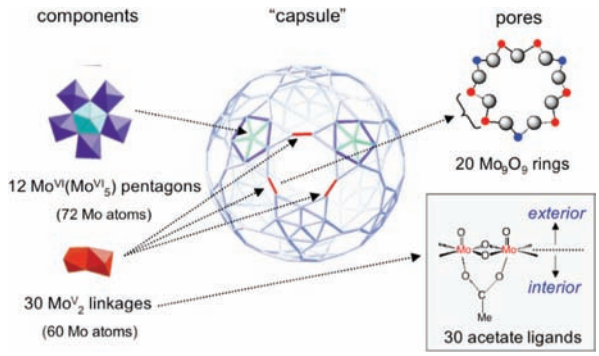

Figure 1. Diagram of the structural building blocks that define the pore structure of "capsule-like" **1**, shown at the center in wireframe notation. At left, Mo(VI) and Mo(V) atoms are located at the center, respectively, of the blue and red polyhedra. Exchangeable acetate ligands (lower right) are bound to the interior surface of the complex via $\eta_2-\mu_2$ coordination to Mo^{V}_2 linkages of the Mo_9O_9 "pores".

Under certain conditions, we now find that the internal carboxylate ligands (RCO_2^-) are in dynamic equilibrium with RCO_2^- anions in solution outside the complex and that increasing the size of the ligands (i.e., of R in RCO_2^-) added to solutions of the capsule decreases the rate at which they begin to occupy internal binding sites. By carefully controlling these processes, we herein document the proton-coupled uptake of carboxylate ligands whose R groups are *larger* than the crystallographic dimensions of the Mo_9O_9 pores.

Stoichiometric quantities of ammonium acetate present in the crystalline lattices of pure samples[4] of $(NH_4)_{42}[\{Mo^{VI}_6O_{21}(H_2O)_6\}_{12}\{Mo^{V}_2O_4(OAc)\}_{30}]\cdot\sim300H_2O\cdot\sim10CH_3COONH_4$—denoted $(NH_4)_{42}$**1**$\cdot\sim300H_2O\cdot\sim10CH_3CO_2NH_4$—(Figure 2, top) were removed, and the NH_4^+ countercations were replaced by Na^+. This was done to avoid possible complications arising from H-bonded associations between NH_4^+ and the negatively charged capsule. It was achieved using a multistep dialysis procedure (see the Supporting Information). Briefly, crystalline $(NH_4)_{42}$**1**$\cdot\sim300H_2O\cdot\sim10CH_3CO_2NH_4$ was dissolved in water, sealed within a regenerated cellulose dialysis membrane (12000 Da cutoff), and stirred at room temperature in an aqueous bath of sodium acetate buffer (4 M; 1:1 H^+/Na^+). After equilibration, the acetate buffer bath was replaced by pure water (six 1 h treatments). The contents of the dialysis tube were then concentrated to dryness by rotary evaporation to give the Na^+ salt of **1** as a dark-red solid (Figure 2, bottom; see Figure S2 in the Supporting Information for ^{13}C NMR spectra). The absence of ammonium acetate and complete replacement of NH_4^+ by Na^+ was confirmed by acid−base titration, FTIR spectroscopy, and elemental analysis, and the integrity of the metal oxide framework of **1** was confirmed by FTIR and Raman[4] spectroscopy (Figures S1, S3, and S4).

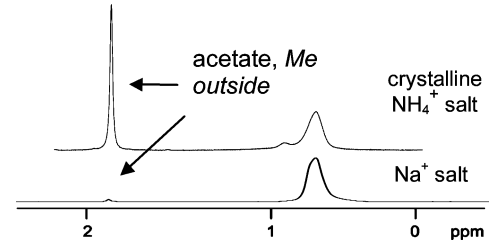

Figure 2. ^1H NMR spectra of $(NH_4)_{42}$**1**$\cdot\sim10CH_3CO_2NH_4$ (top trace) and the Na^+ salt of **1** (bottom trace) in D_2O. The small signal at 1.8 ppm in the spectrum of the Na^+ salt arises from acetate dissociation equilibria, as described in the text. The small broad signal at 0.9 ppm for the NH_4^+ salt is absent in the $MeCO_2NH_4$-free Na^+ salt.

An internal NMR reference (Figure S5) indicated that in solution (50 mg of the Na^+ salt in 0.5 mL of D_2O), 22 acetate ligands are associated with each capsule. This, along with elemental analysis data, give an empirical formula of $Na_{34}[\{Mo^{VI}_6O_{21}(H_2O)_6\}_{12}\{(Mo^{V}_2O_4)_{30}(OAc)_{22}(H_2O)_{16}\}]\cdot\sim300H_2O$ (abbreviated as Na_{34}**2**, with the ~300 H_2O omitted for clarity). The stability data above show that the complex is stable under aerobic conditions in D_2O at its natural pH (~4.5), even with some of the ligands on Mo(V) replaced by D_2O/H_2O.

In solution, ~1 equiv of acetate is observed outside the capsule (see the arrow at the bottom of Figure 2). Because this signal was *always* observed after cation exchange, reversible ligand dissociation

[†] Ben Gurion University of the Negev.
[‡] Institute of Chemical Research of Catalonia.
[§] University of Bielefeld.

10.1021/ja900452d CCC: $40.75

was suspected. To test for this, 86 equiv of CD_3CO_2D was added to a solution of Na_{34}**2** (Figure 3).

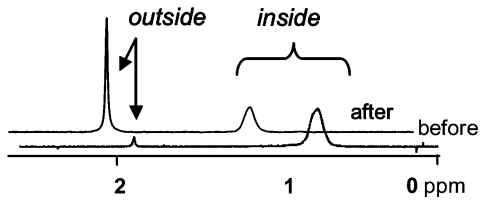

Figure 3. ^{1}H NMR spectra before (bottom trace) and after (top trace) addition of 86 equiv of CD_3CO_2D to a D_2O solution of Na_{34}**2**. Before addition of CD_3CO_2D, the intensity ratio of the methyl-*H* signals is ~0.05 (outside) to 1 (inside). After addition of CD_3CO_2D, most of the $CH_3CO_2^-$ ligands are displaced from the limited number of coordination sites inside the complex, such that the final intensity ratio is 3:1 outside/inside.

Initially, most of the $CH_3CO_2^-$ is located inside the complex (broad signal at ~0.75 ppm). After addition of CD_3CO_2D, most of the methyl protons are observed *outside* the complex. This is consistent with a shift in the equilibrium population of the limited number of coordination sites inside the complex (see page S3 in the Supporting Information for further analysis). This confirms that the signal at 1.8 ppm in Figure 2 (bottom) is due to reversible ligand dissociation in water (eq 1):

$$\left[\{Mo^{VI}{}_6O_{21}(H_2O)_6\}_{12}\{(Mo^{V}{}_2O_4)_{30}(OAc)_{22}(H_2O)_{16}\}\right]^{34-} + 2H_2O \rightleftharpoons \left[\{Mo^{VI}{}_6O_{21}(H_2O)_6\}_{12}\{(Mo^{V}{}_2O_4)_{30}(OAc)_{21}(H_2O)_{18}\}\right]^{33-} + OAc^- \quad (1)$$

Rapid equilibration (before the ^{1}H NMR spectra could be acquired) was also observed when a 1:1 HCO_2Na/HCO_2D buffer was added to Na_{34}**2** in D_2O. As the number of equivalents of 1:1 formate buffer increased, the number of equivalents of acetate inside the capsule decreased, and more formate was observed *inside* the capsule (Figures S6 and S7). At large buffer concentrations, the sum of ligands inside remained constant at ~29. Rapid equilibration was also observed for $EtCO_2D$ and *n*-$PrCO_2D$.

Aliquots of RCO_2D (R = *iso*-Pr, *tert*-Bu, Ph) were then added to D_2O solutions of Na_{34}**2**. In Chart 1, these carboxylates (drawn to scale) are compared with one of the Mo_9O_9 pores in Na_{34}**2** (the space-filling models show van der Waals radii, and the ligands beneath the pore have been omitted for clarity).

Chart 1

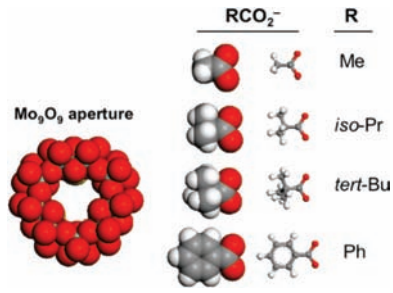

Upon addition of isobutyric acid, which has a branched hydrocarbon chain (R = *iso*-Pr), gradual entry (minutes) accompanied by simultaneous egress of acetate was observed (Figure 4).

Upon addition of 1,1,1-trimethylacetic acid (R = *tert*-Bu, whose diameter is 5.4 Å), the exchange reaction required ~45 days to reach equilibrium (Figure 5). *This result was the same in air or with rigorous exclusion of* O_2. Reactions under both conditions proceeded at the same rate, and no significant differences were observed in the ^{1}H NMR spectra (Figures S9−S11), thus ruling

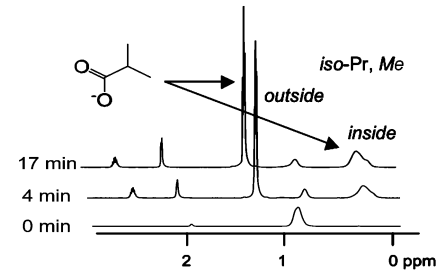

Figure 4. ^{1}H NMR spectra showing the uptake of isobutyrate after addition of 33 equiv (117 mM) of its 1:1 D^+/Na^+ buffer to Na_{34}**2** (3.55 mM) in D_2O. The spectrum at 17 min shows equilibrium signal intensities. The methyl groups on the bound isobutyrate ligand are diastereotopic because of restricted rotation and/or a decrease in symmetry of the complex upon ligand substitution (see Figure S8 for a ^{13}C NMR spectrum of the intact product). The apparent multiplicities in the *Me* (outside) signals are due to imperfect field homogeneity during kinetic analysis (see the text).

out the oxidation of $Mo^{V}{}_2O_4{}^{2+}$ units.[7] In addition, *the Raman bands associated with the molybdenum oxide framework remain unchanged* (Figure S12), thus ruling out irreversible changes in the structure of **2**.

The faster uptake of R = *iso*-Pr (Figure 4) than of R = *tert*-Bu (Figure 5) is consistent with the smaller size of the *iso*-Pr group and its ability to achieve a more sterically favorable orientation relative to the Mo_9O_9 aperture. Because the *tert*-Bu group is larger than the pore opening (on the basis of van der Waals radii), uptake must occur via flexible changes in the bond lengths and angles of the Mo_9O_9 structure and/or other *reversible* changes in the coordination environments of the Mo centers.

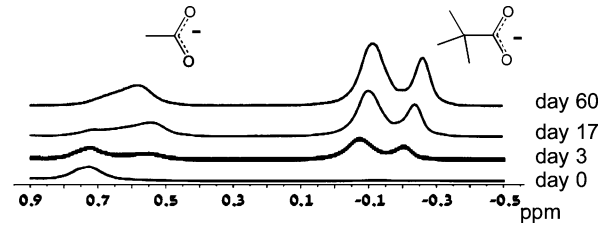

Figure 5. Uptake of 1,1,1-trimethylacetate after addition of 33 equiv (117 mM) of its 1:1 H^+/Na^+ buffer to Na_{34}**2** (3.55 mM) in D_2O. The region shown highlights the decrease in the intensities of the signals for internally bound acetate (0.5−0.8 ppm) relative to the increase in intensities of the signals due to internally bound isobutyrate (ca. −0.3 to 0.0 ppm). A full spectrum is shown is Figure S9.

Finally, for R = Ph, no uptake was observed, even after several weeks of exposure to air. This precludes the possibility that ligand exchange occurs via gross changes in the molybdenum oxide framework but is entirely consistent with size-restricted uptake. In particular, the above trends parallel those for size-restricted diffusion into zeolytes[1,8] and other rigid porous[9] materials: straight chain > secondary > tertiary > phenyl.

Kinetic data were obtained using carefully formulated isobutyrate buffers (R = *iso*-Pr). Uptake of each equivalent of *iso*-$PrCO_2^-$ generates a new and *different* complex (Figure S13). Hence, a sequence of *different reactions* occurs en route to equilibrium. In view of this, ^{1}H NMR spectroscopy was used to determine initial rates, approximated as $\Delta[iso\text{-}PrCO_2^-]_{in}/\Delta t$, where $[iso\text{-}PrCO_2^-]_{in}$ is the concentration of *iso*-$PrCO_2^-$ ligands *inside* the complex after the first 60 s of reaction (i.e., Δt = 60 s). In practice, this corresponded to uptake of ~2−9 *iso*-$PrCO_2^-$ ligands via the 20 equivalent Mo_9O_9 entry sites. Initially, there are 21 bidentate ligand sites occupied by acetate in **2** and nine sites−18 Mo(V)

atoms—occupied by D_2O. As a result, the early stages (first 60 s) of the reaction result primarily in *uptake* of *iso*-$PrCO_2^-$.

First, identical volumes of 1:5 RCO_2D/RCO_2Na (R = *iso*-Pr; in large excess) were added to NMR tubes containing incrementally larger concentrations of Na_{34}**2** in D_2O. The initial rates increased linearly with [Na_{34}**2**] (Figure 6A; $R^2 = 0.998$), and the *y*-intercept was near zero (8×10^{-6} M s^{-1}).

Next, [Na_{34}**2**] was kept constant, and increments of a D_2O solution of 1:5 RCO_2D/RCO_2Na (in excess) were added. The dependence of initial rate on buffer concentration was not linear. Rather, the initial rates increased more steeply at smaller buffer concentrations and appeared to level off at higher ones (Figure S14). The 90 D_2O ligands coordinated to the Mo(V) and Mo(VI) atoms of Na_{34}**2** are weakly acidic. We therefore suspected that as the concentration of added *iso*-$PrCO_2Na$ increased, Brønsted acid−base equilibria[10] between Na_{34}**2** and *iso*-$PrCO_2^-$ might have resulted in a nonlinear increase in the concentrations of *iso*-$PrCO_2D$ actually present in solution.

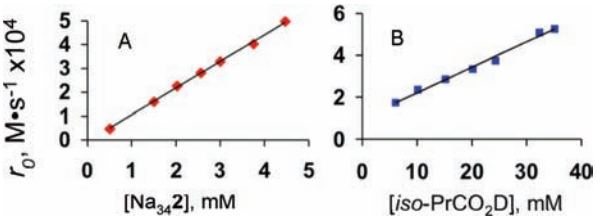

Figure 6. Dependence of initial rates (r_0) in D_2O (A) on [Na_{34}**2**] at fixed [buffer], where buffer = 1:5 D^+/Na^+ forms of *iso*-$PrCO_2^-$ at 0.1059 M (sum of both) and [Na_{34}**2**] was varied from 0.5 to 4.5 mM, and (B) on added [*iso*-$PrCO_2D$] (from 6 to 35 mM) at constant added [*iso*-$PrCO_2Na$] of 0.049 M and constant [Na_{34}**2**] of 3.55 mM.

To control for this, buffer solutions within which concentrations of added *iso*-$PrCO_2D$ increased incrementally at *constant added* [*iso*-$PrCO_2Na$] were used. The results (Figure 6B) revealed a linear (i.e., first-order) dependence of initial rate on [*iso*-$PrCO_2D$]. The *y*-intercept was >0. This suggested that added *iso*-$PrCO_2^-$ was partially converted to its acid form by **2**.[10] Thus at $t = 0$, the concentration of the kinetically competent species, *iso*-$PrCO_2D$, was probably larger than that of *added iso*-$PrCO_2D$ by a constant value.

To verify this, the pH of a Na_{34}**2** solution (3.55 mM) was measured as a function of added *iso*-$PrCO_2Na$ (5 to 55 mM; Figure S15). The pH increased from 4.5 to 5.5, and in D_2O no degradation of **2** was observed by ^1H NMR. In the absence of Na_{34}**2**, the pH increased to >8.7. This clearly demonstrates conversion of *iso*-$PrCO_2Na$ to *iso*-$PrCO_2D$ by **2**.

A near-zero *y*-intercept (5×10^{-10} M see^{-1}) is obtained if only 2.3 D^+ per equiv of **2** (kept constant at 3.55 mM) react with *iso*-$PrCO_2Na$ (initially 49 mM) to convert it to *iso*-$PrCO_2D$. The loss of two D^+ increased the charge of the oxomolybdate from ∼33− to 35−. Because this increase is small (∼6%) and the kinetically competent species (*iso*-$PrCO_2D$) is neutral, the increase in charge should have little effect on the initial rate. Additional evidence that the nonzero *y*-intercept is not due to a parallel pathway involving unprotonated *iso*-$PrCO_2Na$ was provided by the observation that while SO_4^{2-} does not react with Na_{34}**2**, internally bound acetate ligands are rapidly displaced by monodeuterated DSO_4^- (from $NaDSO_4$, final pD ∼1.4; Figure S16). This shows that protonation of the entering ligand is more important than its charge (i.e., neutral vs monoanionic) and suggests that H/D bonding with **2** is responsible for the linear dependence of the rate on [*iso*-$PrCO_2D$].

The plot in Figure 6B is linear even though the kinetically competent species, *iso*-$PrCO_2D$, is not present in large excess. This is because [*iso*-$PrCO_2D$] remains constant throughout the first 60 s of reaction (Figure S17). In other words, *iso*-$PrCO_2D$—the acid form of the ligand—acts as a catalyst. The deuterium cation is released during uptake, and then converts an additional equivalent of *iso*-$PrCO_2^-$ to *iso*-$PrCO_2D$.

The data in Figure 6 give the following rate expression:

$$\frac{d[\textit{iso}\text{-}PrCO_2^-]_{in}}{dt} = k[Na_{34}\mathbf{2}][\textit{iso}\text{-}PrCO_2D] \qquad (2)$$

The slopes of the two plots give respective rate constants *k* (=slope/[Na_{34}**2**] and slope/[*iso*-$PrCO_2D$]) whose values, 3.4 and 5.2 M^{-1} s^{-1}, are in close agreement with one another.

Although the present data do not exclude reversible cleavage of Mo−O bonds, the sensitivity of the rate to the size of R in RCO_2^- points to a more general phenomenon: the greater flexibility of molecular versus solid-state structures. Specifically, the 12 $\{(Mo^{VI})Mo^{VI}_5O_{21}(H_2O)_6\}^{6-}$ pentagons in **2** are linked by 30 $Mo^V_2O_4^{2+}$ spacers, resulting in the presence of 120 Mo^V−O bonds.[5] Small changes in the lengths and angles in this large ensemble of Mo−O bonds could lead to considerable fluctuations in the sizes of the Mo_9O_9 pores and allow for the uptake of species whose sizes are larger than the pore dimensions defined by single-crystal X-ray crystallography.[4]

In summary, a soluble, porous 3 nm diameter capsule was used to demonstrate that large carboxylates can negotiate passage through flexible Mo_9O_9 pore structures *whose crystallographic dimensions are smaller than the sizes of the entering molecules.* Spectroscopic confirmation of stability after reaction under air and N_2, NMR characterization of reaction products, the observation that the rates follow the general trend 1° alkyl ≫ 2° alkyl > 3° alkyl ≫ phenyl (no reaction), and well-behaved bimolecular kinetics provide four independent lines of evidence that the organic ligands enter the interior of the complex through its Mo_9O_9 apertures and that no irreversible changes in the metal oxide framework are involved. The surprising behavior of this molecular open framework likely reflects the greater flexibility of molecular versus solid-state structures and represents a distinct departure from traditional models for diffusion through porous solid-state (rigid) oxide materials.[1,8]

Acknowledgment. We thank the Toman Foundation and ISF 1720/08 (I.A.W.), the Deutsche Forschungsgemeinschaft (A.M.), and Consolider Ingenio 2010 CSD2006-0003 (C.B.).

Supporting Information Available: Materials and methods, Figures S1−S18, and Tables S1 and S2. This material is available free of charge via the Internet at http://pubs.acs.org.

References

(1) Smit, B.; Maesen, T. L. M. *Chem. Rev.* **2008**, *108*, 4125–4184.
(2) Largeot, C.; Portet, C.; Chmiola, J.; Taberna, P.-L.; Gogotsi, Y.; Simon, P. *J. Am. Chem. Soc.* **2008**, *130*, 2730–2731.
(3) Two of many leading references are: (a) Trung, T. K.; Trens, P.; Tanchoux, N.; Bourrelly, S.; Llewellyn, P. L.; Loera-Serna, S.; Serre, C.; Loiseau, T.; Fajula, F.; Férey, G. *J. Am. Chem. Soc.* **2008**, *130*, 16926–16932. (b) Thallapally, P. K.; Tian, J.; Kishan, M. R.; Fernandez, C. A.; Dalgarno, S. J.; McGrail, P. B.; Warren, J. E.; Atwood, J. L. *J. Am. Chem. Soc.* **2008**, *130*, 16842–16843.
(4) Müller, A.; Das, S. K.; Krickemeyer, E.; Kuhlmann, C.; Sadakane, M.; Dickman, M. H.; Pope, M. T. *Inorg. Synth.* **2004**, *34*, 191–200.
(5) Todea, A. M.; Merca, A.; Bögge, H.; van Slageren, J.; Dressel, M.; Engelhardt, L.; Luban, M.; Glaser, T.; Henry, M.; Müller, A. *Angew. Chem., Int. Ed.* **2007**, *46*, 6106–6110.
(6) Schäffer, C.; Merca, A.; Bögge, H.; Todea, A. M.; Kistler, M. L.; Liu, T.; Thouvenot, R.; Gouzerh, P.; Müller, A. *Angew. Chem., Int. Ed.* **2009**, *48*, 149–153.
(7) Merca, A.; Bögge, H.; Schmidtmann, M.; Zhou, Y.; Haupt, E. T. K.; Khaled Sarker, M.; Hill, C. L.; Müller, A. *Chem. Commun.* **2008**, 948–950.
(8) Denayer, J. F.; Souverijns, W.; Jacobs, P. A.; Martens, J. A.; Baron, V. G. *J. Phys. Chem. B* **1998**, *102*, 4588–4597.
(9) Ishii, Y.; Nakayama, N.; Konishi, K. *Chem. Lett.* **2007**, *36*, 246–247.
(10) (a) Liu, T.; Imber, B.; Diemann, E.; Liu, G.; Cokleski, K.; Li, H.; Chen, Z.; Müller, A. *J. Am. Chem. Soc.* **2006**, *128*, 15914–15920. (b) Balogh, E.; Todea, A. M.; Müller, A.; Casey, W. H. *Inorg. Chem.* **2007**, *46*, 7087–7092.

JA900452D